Recombination processes controlling the carrier lifetime in n⁻4H–SiC epilayers with low $Z_{1/2}$ concentrations

P. B. Klein,[1,a] R. Myers-Ward,[1] K.-K. Lew,[1] B. L. VanMil,[1] C. R. Eddy, Jr.,[1] D. K. Gaskill,[1] A. Shrivastava,[2] and T. S. Sudarshan[2]
[1]*Naval Research Laboratory, Washington DC 20375, USA*
[2]*University of South Carolina, Columbia, South Carolina 29208, USA*

(Received 19 April 2010; accepted 18 June 2010; published online 12 August 2010)

The dominant recombination processes controlling the carrier lifetime in n-type 4H–SiC epitaxial layers grown with low concentrations of the $Z_{1/2}$ defect (the dominant bulk lifetime killer), where $Z_{1/2}$ no longer determines the lifetime, have been investigated by studying the variation in the carrier lifetime with temperature. The temperature dependent lifetimes were obtained primarily by low-injection photoluminescence decay for several low-$Z_{1/2}$ epilayers over a wide temperature range. The results were fitted to simulations of the temperature dependent recombination rate, where bulk, surface and interface recombination was considered. No significant contribution from other bulk defects was observed, and upper limits to the bulk recombination rate were found to be consistent with the low $Z_{1/2}$ concentrations measured in these materials. There was also no significant contribution from carrier capture at the epilayer/substrate interface, which is consistent with behavior expected at low injection for low-doped epilayers grown on n^+ substrates. Corresponding high-injection measurements exhibited very different behavior, consistent with the surface/interface under flat-band conditions. Consequently, it is concluded that for low-$Z_{1/2}$ materials, control of the carrier lifetime has not been transferred from $Z_{1/2}$ to another bulk defect, but is instead dominated by surface and interface recombination. Simulations suggest that further enhancement of the total lifetime under the high injection conditions of a device structure would require very thick epilayers, effectively passivated surface and interface recombination and a further reduction in the remaining $Z_{1/2}$ concentrations. The temperature dependence of the low-injection carrier lifetime was also found to provide a method to estimate the surface band bending and the surface defect density. © *2010 American Institute of Physics*. [doi:10.1063/1.3466745]

I. INTRODUCTION

The continuing interest in 4H–SiC as the material of choice for high voltage switching devices derives primarily from its thermal stability, high breakdown field, good transport properties, and high thermal conductivity.[1] While the intense interest in this field over the last decade has led to numerous advances in material quality and in device performance,[2] significant challenges remain to bring this technology to its full potential. An application of particular interest is that of high voltage, bipolar switching devices, where the material properties of 4H–SiC provide a significant advantage over those of Si-based technology.[3] Here, a critical problem area has been the high forward voltage drop that is developed across the thick, low-doped n^- drift region, which leads to excessive heat dissipation when the switch is in the on-cycle. The forward voltage drop is minimized by conductivity modulation, where a high concentration of minority and majority carriers are injected into the drift region under high forward bias, thus raising the conductivity of the layer. However, the concentration of carriers that can be sustained is limited by the minority carrier lifetime, which is controlled by material defects. Thus, high defect concentrations in the drift layer lead ultimately to a high forward voltage drop and high heat dissipation.

Consequently, there has been a significant effort to investigate the nature of defects in this material, and to identify those defects that directly affect the carrier lifetime.[4–10] As a result of this work, it has become apparent that the bulk lifetime in as-grown epilayers is controlled primarily by the $Z_{1/2}$ defect,[4,5,7,9] which is a dominant electron trap approximately 0.62 eV below the conduction band.[11] This defect has been shown to be a–U center[12] that has been identified as V_C-related,[10,13] although the precise local structure of the defect has yet to be determined. Recently, Danno *et al.*[4] have shown that for layers with $Z_{1/2}$ concentrations above $\approx 10^{13}$ cm^{-3}, the recombination rate is proportional to the defect concentration, verifying that this defect controls the carrier lifetime. For $Z_{1/2}$ concentrations below this level, the observed lifetime was found independent of $Z_{1/2}$ concentration, suggesting that *other* recombination processes control the lifetime in these samples. When $Z_{1/2}$ dominates, the lifetime is controlled by Shockley–Read–Hall (SRH) recombination due to carrier capture and emission at deep defects.[14,15] For samples with low $Z_{1/2}$ concentrations, the "other" processes that dominate the lifetime can be due to capture either at other bulk defects, at surfaces, interfaces, or at extended defects.

Due to reductions in the $Z_{1/2}$ concentrations of as-grown material, reproducible low-injection lifetimes in the best epilayers has increased from typically several hundred nano-

[a]Electronic mail: paul.klein@nrl.navy.mil.

seconds to the 2–3 μs range. At higher injection levels, the carrier lifetime will be longer for n-type samples dominated by SRH recombination due to electron traps in the upper half of the band gap.[14] If, however, surface recombination controls the lifetime, then high injection levels can lead to shorter lifetimes, as the surface is driven into flat-band conditions, thus eliminating the surface capture barrier associated with surface band bending that acts to reduce the surface recombination.[4,5,16] While the increased lifetimes observed in low-$Z_{1/2}$ materials are adequate for devices operating at a few kV, longer lifetimes are required for higher voltage devices, as well as for lifetime control.[4,5] Consequently, the nature of the lifetime limiting recombination processes in epilayers with relatively low $Z_{1/2}$ concentrations is of particular current interest.

When the bulk defect concentration is low, the importance of recombination at structural/extended defects must be considered. In materials with particularly high concentrations of structural defects, the carrier lifetime can be dominated by recombination at these sites. Their effects are quite apparent in high-resolution photoluminescence lifetime mapping,[17] acquired with the exciting laser focused to a small spot. In high quality epilayers (grown on low-defect substrates), however, the contribution of these defects to the total recombination rate, while much lower, is not easily assessed, as the defects can vary widely in size, concentration and effective capture cross-section, and can be highly localized, making it difficult to determine their effect on a *bulk* lifetime measurement. While the experimental data that will be presented here suggests the dominance of recombination processes other than $Z_{1/2}$, the extent to which structural defects may contribute is still an open question. In the present study, however, the analysis is confined to bulk, surface, and interface recombination, as these processes adequately account for the observed behavior of the carrier lifetime.

In this work, the recombination processes that control the carrier lifetime in n^-4H–SiC epilayers with low $Z_{1/2}$ concentrations ($<10^{13}$ cm^{-3}) are investigated through a study of the temperature dependence of the lifetime, primarily under low injection conditions. Here we take advantage of the fact that different recombination mechanisms exhibit very different dependences on temperature. The results of the measurements and of simulations of the temperature dependent lifetime indicate that for low-$Z_{1/2}$ materials, control of the carrier lifetime has not been transferred from $Z_{1/2}$ to another bulk defect, but is instead dominated by surface recombination at the sample surface and (for high injection) at the substrate/epilayer interface. A similar conclusion was made by Danno and Kimoto,[4,5] by observing differences in the injection dependence of the carrier lifetime for low- and high-$Z_{1/2}$ material. While the current measurements are in agreement with these observations, it is shown that the direction of this injection dependence is sensitive to temperature and can be entirely reversed with a modest change in either the sample temperature or surface recombination parameters.

In Sec. II we present an analytical model to account for the temperature dependence of the carrier lifetime. The model is based on existing approximations to the solution of the one dimensional diffusion equation, taking into account recombination in the bulk, at the sample surface and at the substrate/epilayer interface. The model provides a useful perspective in interpreting the observed temperature dependences of the carrier lifetime. In subsequent sections, the experimental details are described, followed by the results of temperature dependent lifetime measurements and a discussion of their relevance to the current understanding of recombination in these state-of-the-art materials. The work is summarized in Sec. VI.

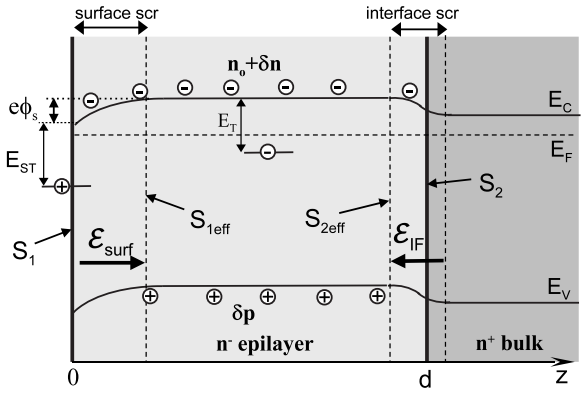

FIG. 1. Schematic energy band profile of an n^- epilayer grown on an n^+ substrate. scrs form at the surface and at the n^+/n^- interface, due to surface defects and to the carrier concentration gradient at the interface, respectively. The resulting band bending leads to significantly reduced effective SRVs at low injection. The surface band bending shown corresponds to surface hole traps, but electron traps and upward band bending also occur.

II. MODEL FOR TEMPERATURE DEPENDENT CARRIER RECOMBINATION

Here, we model the carrier dynamics for a typical n^-4H–SiC epilayer grown on an n^+ substrate under low injection conditions. Figure 1 represents a cross-section of an epilayer with the coordinate z reflecting the depth below the sample surface, with equilibrium carrier concentration n_o, thickness d, surface at z=0 and n^+/n^- interface at z=d. Surface states and/or surface defects are represented by a single trap level of depth E_{ST}, shown in the figure as a hole trap, although an electron trap is also equally possible. Carrier trapping at surface defects creates a space charge region (scr), with band bending $e\phi_s$ at the surface and a surface field $\mathcal{E}_{surf}$ that attracts electrons and repels holes (or the reverse for an electron trap). The surface recombination velocity (SRV) is represented as S_1, and within the neutral region of the epilayer deep electron traps contributing to bulk recombination, such as $Z_{1/2}$, are represented by a level at depth E_T. The surface band bending represents a capture barrier for holes (electrons) diffusing to the surface, thus reducing the effective SRV at the edge of the scr[16,18,19] to $S_{1eff}=S_1 \exp(-e\phi_s/kT)$. This applies whether minority or majority carriers are repelled from the surface (i.e., hole or electron surface trap, downward, or upward band bending), since for recombination both carriers must be captured.

Transfer of electrons from the n^+ substrate to the n^- epilayer at the n^+/n^- interface creates a second scr and an electric field $\mathcal{E}_{IF}$[18,20,21] that repels minority holes, as indicated in Fig. 1. Similar to recombination at the surface, the effective SRV, S_{2eff}, for minority carriers at the edge of the interface

scr[19] is expected to be reduced considerably from the SRV, S_2, at the interface;[18,21] $S_{2eff}=S_2\exp(-\Delta E_{IF}/kT)$, where the magnitude of the potential barrier, ΔE_{IF}, is approximately given by[18,21] $\Delta E_{IF}\cong kT\cdot\ln(n^+/n^-)$. This leads to[20] $S_{2eff}\cong(n^-/n^+)S_2$, which is roughly temperature-independent. Since n^-/n^+ is typically $10^{-3}-10^{-4}$, the magnitude of this reduction is significant, suggesting a dramatic reduction in the effect of the interface on carrier lifetimes at low injection. Consequently, a small S_{2eff} will be a general property of n^-SiC epilayers grown on n^+ substrates under low injection conditions. Reduced SRV at the substrate interface has been observed experimentally in 4H–SiC through free carrier absorption profiling measurements[22,23] at low injection levels. Under high injection conditions, however, the interface recombination was found to be greater than the surface recombination, as high optical excitation results in the flattening of the bands and the elimination or reduction in the carrier capture barriers on both sides of the epilayer. While practical devices operate under conditions of high injection, it is the analysis of both low- and high-injection measurements that provides a means to identify the recombination mechanisms controlling the carrier lifetime.

Modeling of the lifetime through consideration of carrier diffusion and recombination has been considered previously by many authors.[24–27] Consequently, we will only outline some of the major points here. After a short, low-injection excitation pulse, nonequilibrium carrier concentration profiles $\delta n(z,t)$ and $\delta p(z,t)$ are established within the epilayer, with the initial minority carrier distribution $\delta p(z,0)$ determined primarily by the absorption coefficient of the incident light. The problem is approached analytically by assuming that lateral carrier diffusion can be ignored, so that in a homogeneous material with diffusion dominating drift, recombination, and diffusion of excess minority carriers (holes) are described by the one dimensional diffusion equation,

$$\frac{\partial p(z,t)}{\partial t}=D_p\frac{\partial^2 p(z,t)}{\partial z^2}-\frac{p(z,t)}{\tau_{bulk}}, \tag{1}$$

with boundary conditions

$$D_p\frac{\partial p(z,t)}{\partial z}\bigg|_{z=0}=S_1p(0,t),$$
$$D_p\frac{\partial p(z,t)}{\partial z}\bigg|_{z=d}=-S_2p(d,t), \tag{2}$$

and the initial condition immediately after the exciting pulse (neglecting multiple reflections)

$$p(z,0)=(1-R)\Phi_o\alpha e^{-\alpha z}, \tag{3}$$

where D_p is the (injection-dependent) minority carrier diffusion coefficient and τ_{bulk} the bulk carrier lifetime. In Eq. (3), α is the absorption coefficient, R the sample reflectivity, and Φ_o is the photon density of the incident pulse (photon/cm^2).

Applying the boundary conditions, the Fourier series solution[24–27] for p(z,t) is of the form

$$p(z,t)=e^{-t/\tau_{bulk}}\sum_{m=0}^{\infty}B(\cos\alpha_m z+b_m\sin\alpha_m z)e^{-\beta_m t}, \tag{4}$$

where $\beta_m=\alpha_m^2D_p$ and the α_m are determined from the eigenvalue equation

$$\tan(\alpha_m d)=\frac{S_1+S_2}{\alpha_m D_p-\frac{S_1S_2}{\alpha_m D_p}}. \tag{5}$$

The summation in Eq. (4) represents an infinite sum of exponential decay modes, resulting in a nonexponential decay. The solutions to Eq. (5), usually solved numerically, are such that $m\pi\le\alpha_m d\le(m+1)\pi$. Consequently, $\alpha_{m-1}<\alpha_m$ and since $1/\tau_m\sim\alpha_m^2$, a larger m corresponds to a mode with faster decay. Therefore, many values of m are required to describe a very fast initial decay, while for slower decays at later times fewer components are required.[27,28] For long enough times, the m=0 mode is sufficient to describe the decay, which has now become exponential. This mode is generally referred to as the *fundamental mode of recombination.*[27,28] Consequently, for an exponential decay the carrier lifetime can be written as $\tau^{-1}\cong\tau_{bulk}^{-1}+\alpha_o^2D_p$, where the second term reflects the surface contribution to the lifetime and can be evaluated by solving Eq. (5) for m=0.

Sproul[28] has shown that a useful approximate expression for the surface lifetime, $\tau_{surf}=(\alpha_o^2D_p)^{-1}$, can be obtained for the m=0 mode of Eq. (5) by summing the two limiting cases $S\to0$ and $S\to\infty$. The maximum deviation from the exact solution, corresponding to intermediate values of S, was found to be <5%. Ahrenkiel and Dashdorj[29] have extended this, for the case of a stable carrier profile (exponential decay) to take the form

$$\tau_{surf}\cong\frac{(\beta d)^2}{\pi^2D_p}+\frac{d}{S_1+S_2}, \tag{6}$$

where we have included the parameter β; $1\le\beta\le2$. The first term in Eq. (6) reflects the diffusive component of the lifetime (i.e., the limit for large S) and the second the surface capture component (the limit for small S). Since the surface lifetime is the sum of both contributions, the slower of the two processes (with the longest lifetime) will be the rate-limiting process and will dominate the surface recombination. Consequently, if either S_1 or S_2 (or both) is large, the second term in Eq. (6) becomes small and the recombination is diffusion limited. If both SRVs are small, the surface capture term dominates, and $\tau_{surf}\cong d/(S_1+S_2)$.

The first term in Eq. (6) represents τ_{surf} in the limit of large (S_1+S_2). This can occur when both SRVs are large, or when only one SRV is large. Sproul[28] has considered the two extreme limits for large (S_1+S_2), $\beta=1$ and $\beta=2$, which correspond, respectively, to both of the SRVs large and *equal* ($\beta=1$) or to one SRV large and the other approaching zero ($\beta=2$; e.g., $S_1\ll S_2$ or $S_1\gg S_2$). However, there can also be intermediate cases for diffusion limited recombination, where one SRV remains large (S_1, for example) and the other is smaller, but not "very small," e.g., $S_1>S_2$ but not $S_1\gg S_2$. The parameter β has been introduced in Eq. (6), with

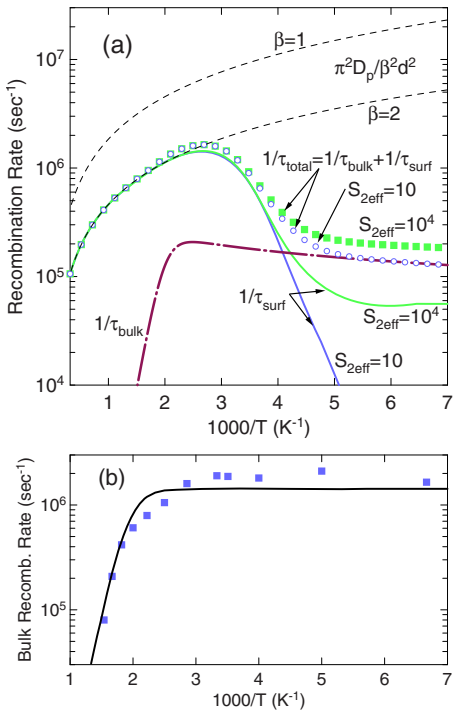

FIG. 2. (Color online) (a) Schematic temperature dependence of the recombination rate for bulk (dotted-dashed line) and surface recombination for $\beta=2$: solid lines for $S_{2eff}=10$ cm/s and $S_{2eff}=10^4$ cm/s. The open circles and filled squares represent the corresponding *total* recombination rates, respectively. The dashed lines indicate the diffusive component for the limiting cases $\beta=1,2$. In the simulations, $d=18$ μm, $e\phi_s=0.25$ eV, $S_1=3.5\times10^7$ cm/s, $E_T=0.55$ eV, and $\tau_{bulk}(T\rightarrow0)=10$ μs. (b) Temperature dependence of the bulk recombination rate for a 160 μm thick layer, where the carrier lifetime is controlled by the $Z_{1/2}$ defect. The solid line is a carrier dynamics simulation for this sample (Ref. 30).

$1\leq\beta\leq2$, in order to represent these intermediate cases for diffusion limited surface recombination.

While Eq. (6) is an approximation to the solution of the surface/interface component of Eq. (4), it provides a useful representation of the temperature dependence of the surface recombination lifetime. The approximation fails at very high values of S_1, which is the regime where the lifetime is already dominated by diffusion, and is less sensitive to the SRV. The temperature dependence of the *measured* lifetime, $\tau_{meas}^{-1}(T)\cong\tau_{bulk}^{-1}(T)+\tau_{surf}^{-1}(T)$, will depend on the temperature variation in the bulk lifetime, the diffusion coefficient and the SRVs. By considering the appropriate temperature dependence of each of these processes, an approximate analytical form for the temperature dependent carrier lifetime can be constructed from Eq. (6) to compare with experiment.

For SRH recombination, the dominant process affecting the temperature dependence of the bulk carrier lifetime is the thermal emission of trapped carriers, which leads to a thermally activated increase in the lifetime,[30] with the activation energy E_T reflecting the depth of the trap. Assuming no temperature dependence for the carrier capture cross-sections, at lower temperatures only the $T^{1/2}$ variation in the carrier thermal velocity contributes significantly. A typical temperature dependence for bulk recombination, $\tau_{bulk}^{-1}(T)$, is shown schematically in Fig. 2(a) as the dashed-dotted line, and an experimental example for a thick (160 μm) layer dominated by recombination at the $Z_{1/2}$ bulk defect is shown in Fig. 2(b), where the solid curve represents a carrier dynamics simulation for that sample.[30]

The temperature dependence of the diffusion coefficient can be related to the temperature dependent mobility through the Einstein relations: $D_p(T)=kT\mu_p(T)/e$. As Grivickas *et al.*[31] have pointed out, determining $D_p(T)$ in n-type material from $\mu_p(T)$ measured by Hall effect in p-type material is problematic, because the temperature dependence of the Hall factor in p-type 4H–SiC is not known. Their high-injection measurements found that the temperature dependence of the *ambipolar* diffusion coefficient in n$^-$4H–SiC varied as $T^{-1.3}$. We will assume a similar temperature dependence here for the minority carrier diffusion coefficient;

$$D_p(T)=D_{300}\left(\frac{300}{T}\right)^{1.3}. \tag{7}$$

D_{300} is the room-temperature diffusivity, measured by Grivickas *et al.*[31] as a function of injection level. At the injection employed here, $\approx2\times10^{14}$ cm^{-3}, $D_{300}\cong2.8$ cm^2/s.

The temperature dependence of the surface recombination velocity S_1 derives primarily from the surface band bending resulting from trapped surface charge (Fig. 1). As noted earlier, the band-bending can act as a capture barrier to nonequilibrium carriers diffusing to the surface,[16,18] thus reducing the SRV to an effective SRV at the edge of the scr. This is represented by $S_{1eff}(T)$, and takes the form[16,18,19,32]

$$S_{1eff}(T)=S_1e^{-e\phi_s/kT}, \tag{8}$$

where $e\phi_s$ is the band bending and S_1 is the SRV at the sample surface. This temperature dependence is different from that for the SRV at the epilayer/substrate interface because (as noted above) the presence of the scr resulting from the n^+/n^- interface leads to temperature-dependent band bending, ΔE_{IF}, that effectively cancels out the temperature dependence of S_{2eff}.

With $S_{1eff}(T)$ and S_{2eff} replacing S_1 and S_2, respectively, Eq. (6) can be written as

$$\tau_{surf}(T)\cong\frac{(\beta d)^2}{\pi^2D_{300}}\left(\frac{T}{300}\right)^{1.3}+\frac{d}{S_1e^{-e\phi_s/kT}+S_{2eff}}. \tag{9}$$

Equation (9) provides an expression that can be compared directly to experiment. One process *not* represented in Eq. (9) is the thermalization at high temperature of carriers trapped at deep surface traps. This re-emission of trapped carriers back into the bands will lead to an exponential increase in the carrier lifetime with increasing temperature, with activation energy E_{ST} (Fig. 1). The manifestation of this effect at high temperatures on $1/\tau_{surf}(T)$ will be a rapid, exponential downturn in $1/\tau_{surf}$ with increasing temperature, which is observed in one of the samples studied here.

Using Eq. (9), $\tau_{surf}^{-1}(T)$ is plotted schematically as the solid lines in Fig. 2(a) with typical parameter values and with $S_{2eff}=10$ cm/s and $S_{2eff}=10^4$ cm/s. $\tau_{surf}^{-1}(T)$ is compared in the figure to the very different temperature dependence of the

TABLE I. Material parameters (layer thickness d, doping n_o, $Z_{1/2}$ concentration, and off-cut angle), fitting parameters to Eq. (9) ($e\phi_s$, β, and S_1), SRV at 300 K and surface defect density n_s for the six 4H–SiC samples.

	NRL-1	NRL-2	NRL-3	USC-1	USC-2	USC-3
d(μm)	18	18	35	19	21	20
$n_o(10^{15}\ cm^{-3})$	1	9	0.7	6	5	1.5
$[Z_{1/2}](10^{12}\ cm^{-3})$	1.3	1.7	1.3	3.6	0.5–1	1.2
Off-cut angle (deg)	8	8	4	8	8	8
$e\phi_s$ (eV)	0.25	0.25	0.28	0.23	0.28	0.27
β	1.9	1.7	1.3	1.5	≈1.6	1.5
$S_1(10^7\ cm/s)$	4.5	11	25	2.5	≈2.0	2.8
S_{1eff}(300 K) (cm/s)	2840	6940	4940	3420	≈400	570
$n_s(10^{10}\ cm^{-2})$	4.9	15	4.4	11	12	6.2

inverse bulk lifetime, τ_{bulk}^{-1} (dotted-dashed line). At low temperature, when $S_{1eff}(T)+S_{2eff}$ is not large and $S_{2eff} \ll S_{1eff}$, surface recombination is dominated by surface capture, with $1/\tau_{surf} \cong S_1 \exp(-e\phi_s/kT)/d$ increasing exponentially with increasing temperature. At higher temperature, $S_{1eff}(T)$ becomes large, resulting in diffusion-limited recombination, with τ_{surf}^{-1} decreasing slowly with increasing temperature, following the diffusion coefficient $\sim T^{-1.3}$, as indicated in Fig. 2(a). The peak in $\tau_{surf}^{-1}(T)$ versus T^{-1} results from the opposite temperature dependences of the two terms in Eq. (9). The total recombination rate, $\tau_{total}^{-1}=\tau_{bulk}^{-1}+\tau_{surf}^{-1}$, is plotted as the open circles ($S_{2eff}=10$ cm/s) or solid squares ($S_{2eff}=10^4$ cm/s) in Fig. 2(a). The diffusive component of the inverse surface lifetime, $\pi^2 D_p(T)/(\beta d)^2$, is plotted in the figure as the dashed lines for the two limiting values $\beta=1$ and $\beta=2$.

It is evident that for $S_{2eff} \ll S_{1eff}$ and for $\tau_{bulk}^{-1} \ll \tau_{surf}^{-1}$, the total low temperature recombination rate is dominated by surface capture, and will increase exponentially with increasing temperature. However, at low temperature a substantial contribution from either bulk or interface recombination (both slow-varying with temperature) will dominate over the Arrhenius behavior associated with the surface band bending [as shown in Fig. 2(a)]. Consequently, a slow-varying lifetime at low temperature is indicative of significant bulk or interface recombination. In cases where $\tau_{bulk}^{-1} > {}^{-1}_{surf}$, the temperature dependence of the total recombination rate will be dominated by capture at bulk defects, similar to that shown in Fig. 2(b). The Arrhenius behavior of τ_{surf}^{-1} will be masked in this case as well.

III. EXPERIMENTAL

Six 4H–SiC epilayers were studied; three grown at Naval Research Laboratory (NRL) and three at University of South Carolina (USC). The layers had relatively low $Z_{1/2}$ levels and carrier concentrations were in the range $\approx(1-9)\times10^{15}$ cm^{-3} (see Table I). The samples were investigated primarily by time-resolved photoluminescence (TRPL) at a low level of injection ($\approx 2\times10^{14}$ cm^{-3}). High injection conditions were investigated by TRPL and transient free carrier absorption (TFCA) measurements.

NRL samples were grown in an Aixtron VP508 horizontal hot-wall reactor using the standard chemistry of silane (2% in H_2) and propane, while Pd-purified hydrogen was used as the carrier gas. Substrates were commercially obtained (0001) 4H–SiC. Two samples were grown on 8° off-cut and one on 4° off-cut substrates toward.[11–20] All films were grown at 1580 °C, 100 mbar, and C/Si=1.55. Propane was introduced during the ramp to growth temperature at 1400 °C to maintain smooth morphology. The films were intentionally doped ($<1\times10^{16}$ cm^{-3}) using an ultra high purity nitrogen source gas.

The epitaxial growth of the USC samples was carried out in a home-built, vertical-hot-wall chemical-vapor deposition chamber. Temperatures between 1400–1650 °C were used during epitaxial growth, with the chamber kept at 300 Torr. Propane and dichlorosilane were used as precursor gases, while hydrogen was used as the carrier gas. In this study, commercial 4H–SiC (0001) substrates all off-cut 8° toward[11–20] were used.

The measured lifetimes were determined from the exponential decay of the band-edge photoluminescence (PL) peak at 391 nm. The PL was excited at 355 nm by a frequency-doubled, cavity-dumped Ti:sapphire laser generating <150 fsec pulses at 40–1000 kHz with average pulse energy of ≈5 nJ. The emitted light was analyzed by a 1/4-m. double spectrometer and detected by a cooled GaAs photomultiplier and time-correlated single photon counting. For temperatures ≥300 K the sample was placed on a temperature-regulated heat stage, while for temperatures ≤300 K a flow-through optical cryostat was used. High-injection PL measurements were excited at 355 nm by a frequency-tripled Nd:$Y_3Al_5O_{12}$ laser generating ~4 ns pulses at 10–30 Hz. TFCA measurements employed the same excitation source and were probed by a 1300 nm cw diode laser. The transmitted probe beam was detected by an InGaAs photodiode coupled to a fast transimpedence amplifier and acquired by a digital oscilloscope.

A Sula Technologies deep-level transient spectroscopy system was employed to measure the dominant electron trap concentrations of the $Z_{1/2}$ defects, scanning from 250 to 350 K and using initial delays of 50, 20, 10, and 5 ms. Nickel Schottky diodes with a diameter of 1000 or 1500 μm (depending upon the electron concentration necessary to produce similar background capacitance values) were deposited by electron beam evaporation on shadow masked samples.

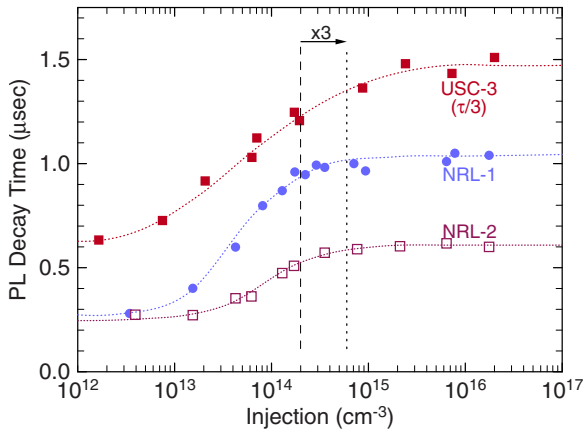

FIG. 3. (Color online) Injection dependence of the carrier lifetime for three n^- epilayers near room temperature. The dashed line indicates the injection level used in the measurements, while the dotted line is at three times this level, simulating the injection level at 650 K (see Appendix). The increase in the carrier lifetime due to the temperature-dependent absorption coefficient is ≤10% over the entire temperature range. The solid lines represent spline fits to the data. For USC-3, 1/3 of the lifetime is plotted.

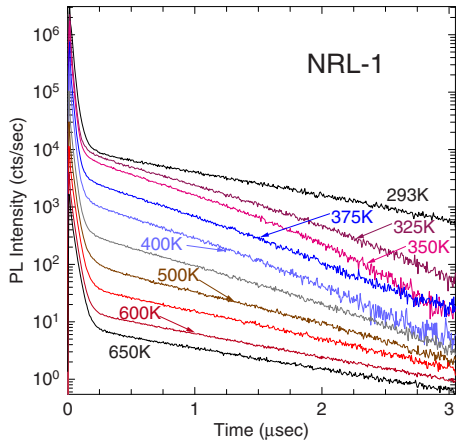

FIG. 4. (Color online) TRPL decays of the 391 nm near-band-edge emission for sample NRL-1 between 293 and 650 K. The carrier lifetime at the incident injection level is reflected in the initial slope of the slow component of the decay. Temperature intervals are 25 K between 325 and 400 K and 50 K thereafter.

IV. RESULTS

A. Temperature dependent injection level and measured lifetimes

Temperature dependent measurements can often be challenging, because many material parameters can vary simultaneously with the varying temperature. In the present case, the carrier lifetimes are sensitive to injection level, and the injection level itself depends on the absorption coefficient of the incident light. Since the absorption coefficient is temperature-dependent, this can lead to variations in the measured lifetime with varying temperature that are simply manifestations of the change in injection level, rather than any inherent dependence of the lifetime on temperature. Since the latter is the focus of this work, it is important to estimate the magnitude of this effect in order to determine whether the measured lifetimes are significantly affected by the temperature variation in the carrier injection. It is shown in the Appendix that over the temperature range of the measurement, this effect leads to a variation in the carrier lifetime of ≤10%. This increase, distributed over the entire temperature range, is not considered to be sufficient to cause a serious distortion of the temperature-dependent carrier lifetimes, as the measured temperature variations discussed in Sec. IV B are considerably larger than this.

Since the carrier lifetime is highly sensitive to both temperature and injection level, it is useful to first obtain a sense of how the lifetime is varying with injection level for the group of samples studied here. The dependence of the room-temperature lifetime on injection level, in the range $\approx 2 \times 10^{14}$ to 2×10^{16} cm^{-3}, is shown in Fig. 3 for three samples: NRL1, NRL2, and USC3. It is interesting that the carrier lifetimes increase with increasing injection. This is similar to what is observed for SRH recombination in these materials.[30] For surface recombination, this dependence would correspond to a SRV that decreases with increasing injection. This behavior is not always representative of surface recombination, however, as the injection dependence of the SRV is sensitive to several parameters, including the ratio of capture cross sections for electrons and holes at surface traps, the initial surface band bending $e\phi_s$, (i.e., surface charge), the energy position and/or distribution of surface traps and the doping level.[33–35] At higher injection (well beyond the range of Fig. 3) the surface lifetime can decrease with injection (when surface capture dominates over carrier diffusion—see Sec. V), as the photoinjected carriers screen the surface charge density, thus collapsing the surface depletion layer and enhancing the surface capture rate of nonequilibrium carriers, as the surface is driven into flat-band conditions. This increase in surface capture rate can also occur at low injection, if the temperature is raised sufficiently for carriers to overcome the capture barrier created by the surface band bending [e.g., Eq. (8)].

B. Temperature-dependent lifetime measurements

The temperature dependence of the PL decay at low injection between 293 and 650 K is shown for sample NRL-1 in Fig. 4, and is representative of the group of samples studied here. The decays have been shifted vertically to enhance the clarity of the figure. While the fast initial decay at low injection can contain contributions from higher-order surface recombination [Eqs. (4) and (5)] and from the n^+ substrate, it is dominated by an artifact—background radiation believed to emanate from the frequency doubling crystal. The near-band-edge epilayer emission, centered near 391 nm, is represented by the slow decay component, as verified by time-resolved PL spectra. Several of the decays at the lower temperatures exhibit a reduced lifetime at later times—an indication that the lifetime decreases with decreasing excess carrier concentration, as in Fig. 3. The initial slope of the slow component reflects the lifetime associated with the initial injection level of the experiment, $\approx 2 \times 10^{14}$ cm^{-3}. It is clear that as the temperature is raised above 293 K, this carrier lifetime decreases. Above approximately 375 K, however, the lifetime begins to increase with increasing temperature. This general behavior was characteristic of the samples

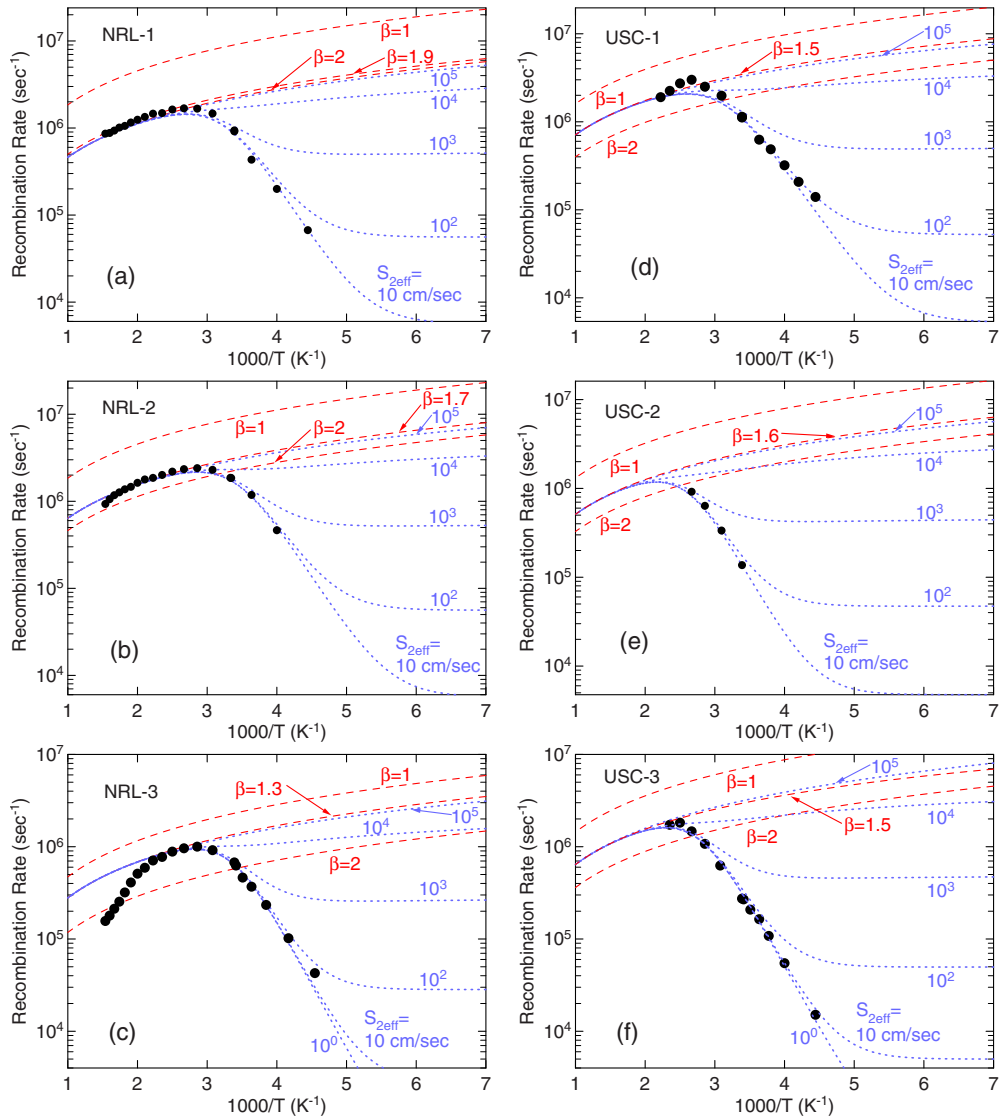

FIG. 5. (Color online) Temperature dependence of the measured recombination rate (filled circles) for the six samples studied in this work. Dashed lines reflect the diffusive component of the surface recombination rate for $\beta=1,2$ and for the intermediate value of β determined from the fit of the data to Eq. (9). The dotted curves indicate the best fit of the data to the surface recombination rate [Eq. (9)] as well as the effect of varying S_{2eff} over a wide range.

studied here. The measured temperature dependence of the recombination rate (inverse lifetime) for all six samples is shown as the solid circles in Figs. 5(a)–5(f).

The temperature range of the available data in Fig. 5 is somewhat different for each sample, as reliable lifetime measurements were not always possible over the entire temperature range for some of the samples, due to interference from temperature-dependent background PL or from slow detrapping from deep trapping centers at the higher temperatures.[36] The general shape of τ^{-1} versus T^{-1} for all of the samples is similar to the temperature-dependent surface recombination rate [Eq. (9)] shown as the solid line ($S_{2eff}=10$ cm/s) in Fig. 2(a). At low temperature, all of the samples exhibited thermally-activated increases in $1/\tau$ as the temperature was increased. This is consistent with surface recombination when surface capture dominates over diffusion (i.e., low temperature) and when S_{2eff} is small (expected for low injection), as discussed in Sec. II in relation to Eqs. (8) and (9) and Fig. 2(a). At high temperature, $1/\tau$ decreases slowly with increasing temperature, generally following the power law temperature dependence of the diffusivity, as the diffusive term in Eq. (9) becomes dominant in this temperature range. The dashed lines in Fig. 5 represent the temperature dependence of the diffusive component of the surface lifetime [see Eq. (9)] for the two limiting cases, $\beta=1$ and $\beta=2$, as well as for the intermediate value of β that best fit the experimental data.

The dotted lines represent simulations of the surface recombination rate [Eq. (9)] for the best-fit parameter values (β, $e\phi_s$, and S_1, see Table I) and for a wide range of S_{2eff} (10^0 to 10^5 cm/s). The resulting 300 K values for S_{1eff} [using Eq. (8)] are also included in Table I. It is apparent from the figure that only small values of S_{2eff} ($\leq 10^2$ cm/s) are consistent with the experimental data. At low temperatures, the observation of thermally activated behavior is possible only if S_{2eff} is small and if the bulk recombination rate is small [see Fig. 2(a)], as both of these contributions are slow-varying and would otherwise dominate over the Arrhenius behavior in this temperature range, where the surface recombination rate is decreasing exponentially with lower tempera-

ture. Also, as a result of the limited range of available data for sample USC-2, there is significant uncertainty in the fitting parameters S_1 and β in Table I for this sample. However, the thermally activated behavior of the recombination rate is still quite clear in this case.

It is apparent from these observations that surface recombination alone can account for the major temperature variations in the carrier lifetime. Evidence of this can also be seen in the high temperature measurements, where $1/\tau$ should fall inside the region between the two dashed curves in Fig. 5 that correspond to the two limiting cases ($\beta=1$ and $\beta=2$) for diffusion-limited surface recombination. It is apparent from Fig. 5 that this is the case for all six samples that were studied. Since these two limits depend only on the layer thickness and the diffusion coefficient, there are no adjustable parameters to force the data into this "allowed" region. The fact that the high-temperature data is observed to fall in the region between the two extreme values of β further supports the conclusion that surface recombination dominates in these samples.

The high-temperature behavior of sample NRL-3 [Fig. 5(c)] is somewhat different than the others, in that the slow increase in lifetime with increasing temperature above ≈350 K ($1000/T<2.86$), apparently following $D_p(T)$, rapidly becomes an exponentially increasing lifetime above ≈450 K ($1000/T<2.22$). This rapid increase in lifetime with temperature is characteristic of the thermal emission of carriers trapped on deep surface defects—a process discussed in Sec. II but not specifically included in Eq. (9). The observed Arrhenius behavior corresponds to a thermal activation energy of ≈0.25 eV. As this was the only sample grown on a 4° off-cut substrate, it is possible that this defect is related to the 4° surface.

The measured carrier lifetimes have been obtained at a relatively low level of injection. It is a result of these low-injection conditions that the Arrhenius behavior, resulting from surface band bending, is observed at all. High injection will result in flat-band conditions, which will lead to the disappearance of the exponential increase in recombination rate with temperature and a decrease in the lifetime. This behavior was observed experimentally (for injections between 4×10^{17} and 3×10^{18} cm^{-3}) and is shown for sample NRL-1 in Fig. 6. The low-injection TRPL data from Fig. 5(a) is shown as the open circles, while high-injection TRPL data appears as the filled circles. Comparable TFCA measurements at the same high injection level are represented by the filled squares. The factor of two longer lifetime for the TFCA measurement results from the bimolecular recombination of the PL emission at high injection.[30] The dramatic reduction in lifetime at low temperature and the disappearance of the Arrhenius behavior under flat-band conditions is readily apparent, and further supports the dominance of surface recombination in these materials. While Auger recombination can become important at the highest injection level employed (3×10^{18} cm^{-3}), similar results were observed at an order of magnitude lower injection. Also, as the Auger coefficient is highly temperature dependent, decreasing with temperature by more than an order of magnitude[37] over the temperature range employed here, a significant Auger contribution would lead to a strong temperature dependence for the high injection data in Fig. 6.

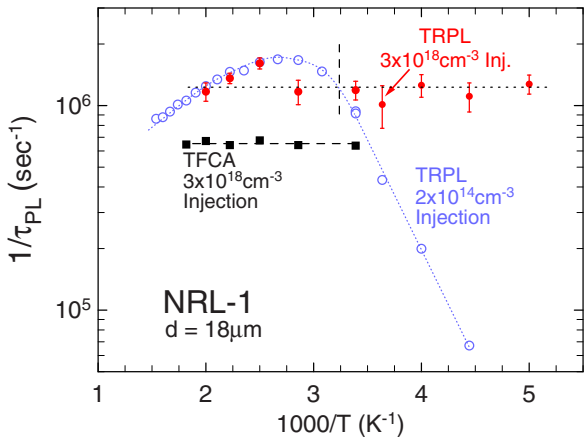

FIG. 6. (Color online) Temperature dependent recombination rate for sample NRL-1 from TRPL at low injection (open circles) and at high injection (filled circles). The filled squares reflect TFCA measurements at the same high injection. At temperatures below ≈310 K (vertical dashed line), where the surface lifetime is dominated by surface capture, increasing the injection level from low-to high-injection results in a decrease in the carrier lifetime. Above this temperature, an increase in the lifetime can be observed.

V. DISCUSSION

In this work we have investigated the recombination processes that control the carrier lifetime in materials where the $Z_{1/2}$ defect concentration is low, so that the lifetime is controlled by other bulk defects, surface/interface recombination, or structural defects. The latter was removed from consideration by focusing on bulk lifetime measurements on epitaxial layers grown on high-quality substrates. The temperature dependence of the carrier lifetime was measured to distinguish between the remaining possible recombination processes. As noted in Sec. IV, the experimental data suggests that it is surface recombination that dominates the carrier lifetime for all of the low-$Z_{1/2}$ samples that were studied. This conclusion is based upon; (1) the agreement between the experimental data and the simulations [Eq. (9)] for temperature-dependent surface recombination in Fig. 5; (2) observed high temperature recombination rates that fall in between the allowed values of $1\leq\beta\leq2$ for surface recombination, with no adjustable parameters; (3) the disappearance of the thermally activated low-temperature recombination rate at high injection; and (4) the lack of any observed contribution from bulk defects.

The contribution from bulk defects should be very apparent at low temperature. As shown in Figs. 2(a) and 2(b), at low injection the low-temperature behavior of $1/\tau_{bulk}$ is slow-varying (as is interface recombination), while the surface recombination rate is decreasing exponentially with lower temperatures. Consequently, the *total* recombination rate would be dominated by the bulk and/or interface components at low temperatures, unless the bulk and/or interface lifetimes are particularly long. From the data in Fig. 5, it is apparent that with decreasing temperature there is no evidence that the exponentially decreasing recombination rate is

"flattening out" toward a constant value, which is expected for dominant bulk or interface recombination. From the minimum measured low-temperature recombination rates in Fig. 5 for all six samples, a *maximum* bulk recombination rate can be estimated. This is in the range $1/\tau_{bulk} < (10^4 - 10^5\ s^{-1})$ for this group of samples, corresponding to $\tau_{bulk} > 10-100\ \mu s$. With $1/\tau_{bulk} = \sigma_p v_{th} N_{Z1/2}$, hole capture cross-section[9] $\sigma_p \approx 5 \times 10^{-15}\ cm^2$ and the minority carrier thermal velocity $v_{th} \approx 1 \times 10^7\ cm/s$, this range of minimum bulk lifetimes corresponds to $Z_{1/2}$ concentrations $N_{Z1/2} < (0.2-2) \times 10^{12}\ cm^{-3}$, which is in very good agreement with the measured defect concentrations in Table I. Consequently, the association of the observed temperature dependence with surface recombination and the lack of significant bulk recombination are consistent with the measured bulk $Z_{1/2}$ concentrations in these samples.

It is apparent, then, that the lifetimes of minority carriers in these low-$Z_{1/2}$ epilayers are dominated by surface recombination, with the contribution from bulk defects consistent with the existing low levels of the $Z_{1/2}$ defect. It might appear that subsequent efforts to enhance the carrier lifetime would have to focus on the properties of surfaces and interfaces, rather than on reducing the concentration of bulk defects. However, in an operating device, the injection level in the drift region is high and the temperature is elevated. Consequently, the SRVs at both the surface and the substrate interface will be at a maximum, and the surface lifetime at a minimum, determined primarily by carrier diffusion ($S \rightarrow \infty$): $\tau_{surf} = \tau_{min}(T) = d^2/\pi^2 D_p(T)$. The *total* lifetime in the drift region of such a device is $\tau_{total} = (\tau_{min}^{-1} + \tau_{bulk}^{-1})^{-1}$. To attain carrier lifetimes in excess of, e.g., 10 μs at device operating temperature, requires that both surface and bulk lifetimes are *each* longer than 10 μs. The total lifetime τ_{total} is plotted in Fig. 7 as a function of epilayer thickness for temperatures between 300 and 600 K, both for infinite bulk lifetime (solid curves) and for a bulk lifetime of 10 μs (dashed curve). It is apparent that to achieve long lifetimes, very thick epilayers are required with $\tau_{bulk} > 10\ \mu s$. Consequently, as the lifetimes for $T \geq 300$ K of materials studied here were considerably shorter than this, it is evident that in addition to reduced surface/interface recombination rates, further reductions in the $Z_{1/2}$ defect concentration will also be necessary. These observations assume that at high injection the unscreened SRVs S_1 and S_2 are large. To see the effect of reduced SRVs, in the inset of Fig. 7 the total lifetime is again plotted against layer thickness for infinite and for 10 μs bulk lifetimes, but with T=400 K and a range of SRVs, $S = S_1 + S_2$. It is clear from the figure that for $\tau_{bulk} > 10\ \mu s$ substantial increases in the total lifetime are possible in thick layers if the unscreened SRVs can be reduced to $\leq 10^3\ cm/s$. Consequently, prospects for enhanced carrier lifetimes in device structures would appear to require thick epitaxial layers, rather substantial progress in reducing defect densities at the surface and substrate interface, and further reductions in the $Z_{1/2}$ defect concentration. However, at such low $Z_{1/2}$ concentrations it is certainly possible that control of the *bulk* lifetime could be taken over by other bulk defects or by structural defects, thus limiting the carrier lifetime. Furthermore, if injection levels in a device become high enough to activate

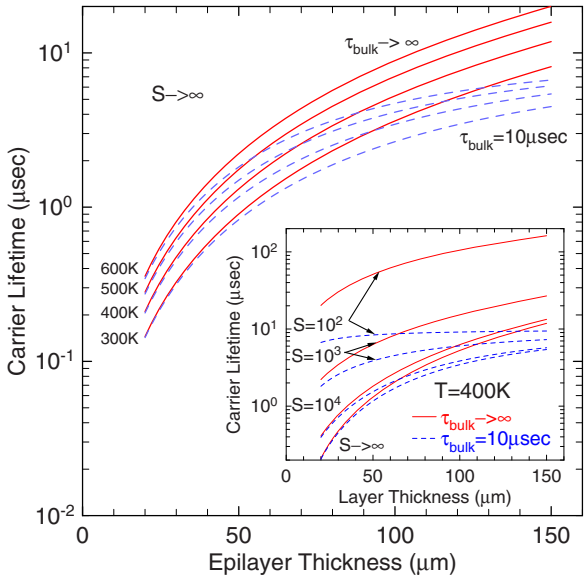

FIG. 7. (Color online) The simulated total carrier lifetime is plotted as a function of epilayer thickness for temperatures between 300 and 600 K assuming the high injection conditions (large S_1+S_2) appropriate for a device structure. The solid curve corresponds to infinite bulk recombination lifetime, while the dashed curve corresponds to a bulk lifetime of 10 μs. The inset shows a similar dependence for T=400 K and a range of unscreened SRVs; $S = S_1 + S_2$.

significant Auger recombination, this process would then take over as the lifetime-limiting recombination mechanism, again leading to significantly shorter carrier lifetimes.

It was shown in Fig. 6 that the temperature dependence of the surface recombination rate varies strongly with injection, as the band bending at the surface and at the n^+/n^- interface disappears at high injection. This leads to an increased SRV at high injection that is generally associated with a decrease in the carrier lifetime, which is opposite to the injection dependence expected from SRH recombination in SiC. It is noteworthy that the vertical dashed line in Fig. 6 near room temperature ($\approx$310 K) roughly separates the region (lower temperature) where increasing from low to high injection leads to shorter lifetimes, from the region (higher temperatures) where increasing to high injection leads to longer lifetimes. These correspond roughly to surface-capture-dominated and diffusion-dominated surface recombination, respectively. This behavior is very different from SRH recombination, where the latter temperature dependence is observed in n-type 4H–SiC.[14,30,38] The temperature at which this transition occurs (denoted T_X) can vary significantly between samples, depending on S_1, $e\phi_s$, β, and d. Danno and Kimoto[4,5] observed for low-$Z_{1/2}$ samples a reduction in the room-temperature carrier lifetime with increased injection, leading to the conclusion that surface recombination controlled the lifetime, in agreement with the current results. For this injection dependence to be observed, however, the surface lifetime must be dominated by surface capture, i.e., $T < T_X$. If, for example, such a measurement were carried out for sample NRL-1 in Fig. 6 at slightly higher temperature, or if T_X were slightly lower, the carrier lifetime might increase with injection, rather than decrease. It should also be noted that the increase in lifetime with injection in-

dicated in Fig. 3 is at much lower injection levels that are incapable of inducing flat-band conditions. This injection dependence results from totally different physical processes, as discussed in Sec. IV A.

From the fit of the experimental data to Eq. (9), a measure of the band bending, $e\phi_s$, was obtained (Table I). From this and the measured equilibrium carrier concentration for each of the samples, an estimate of the density of carriers trapped on surface defects can be determined (Table I) employing the approach of Kingston and Neustadter.[39] The range of defect densities for the six samples studied was found to be $(4-15)\times 10^{10}$ cm^{-2}, as indicated in the table. The measurement of the temperature dependence of the carrier lifetime at low temperature thus represents a potential method for estimating the surface band bending and the surface defect density. This procedure depends upon the measurement being carried out at low injection and upon the fact that the n^- epilayer is grown on an n^+ substrate, so that the resulting scr at the substrate interface insures that the interface SRV does not contribute significantly to recombination, leaving only the thermally activated surface component. A related technique was used by 't Hooft and van Opdorp in AlGaAs heterostructures to determine the temperature-dependent SRV.[40]

VI. SUMMARY

The temperature dependence of the carrier lifetime has been measured in n^-4H−SiC epilayers with low $Z_{1/2}$ concentrations grown on n^+ substrates, in order to investigate the recombination processes controlling the lifetime when $Z_{1/2}$ defects no longer dominate. The measurements have been compared to simulations of the temperature-dependent surface and bulk recombination rates. No evidence of significant bulk recombination was observed above the 10^4-10^5 s^{-1} range, which was found consistent with the bulk ($Z_{1/2}$) defect concentrations. The experimental results were found to follow the behavior expected for surface recombination, exhibiting a thermally activated increase in the recombination rate at lower temperatures, where surface capture dominates over diffusion. The Arrhenius behavior results from surface band bending acting as a capture barrier for excess carriers, and applies only to low injection conditions, since at high injection, flat-band conditions prevail and the surface/interface band bending disappears. At high temperatures, the recombination rate generally followed the temperature dependence of the minority carrier diffusion coefficient. The thermally activated recombination rate at low injection was also found to provide a method for estimating the surface band-bending and surface defect concentrations for epilayers grown on n^+ substrates.

The observation of a thermally activated surface recombination rate at low temperature is not expected if there is significant contribution from bulk or interface recombination. The interface recombination rate was found to be small within the temperature range of the measurements, due to the existence of the n^+/n^- interface. The interface forms a scr that repels minority holes originating in the neutral region of the epilayer, thus dramatically reducing the effective SRV at the edge of the scr. These results apply only to low-injection conditions, since at high injection the interface is driven to flat-band conditions and the SRV is at a maximum.

Considering the effects of high injection and elevated temperature present in an active device, the results of simulations suggest that improvement in the carrier lifetime of the drift region above the 10 μs range will require very thick epilayers, substantial improvement in the surface and interface SRVs and still lower $Z_{1/2}$ concentrations.

ACKNOWLEDGMENTS

The authors would like to thank J. Caldwell and O. Glembocki for kindly carrying out supporting optical characterization measurements. Work at the Naval Research Laboratory is partially supported by ONR. KKL and BLV acknowledge the support from the ASEE-NRL Postdoctoral Fellows Program.

APPENDIX: EFFECT OF TEMPERATURE DEPENDENT INJECTION ON MEASURED LIFETIMES

It was noted in Sec. IV A that the temperature-dependent absorption coefficient leads to a temperature-dependent injection level, so that some of the variations in carrier lifetime with temperature may simply result from a varying injection level rather than any inherent dependence of the lifetime on temperature. To assess the magnitude of this effect, it is first necessary to define how the injection level itself is determined. As is evident from Eq. (3), the initial distribution of injected carriers below the sample surface is exponential, so the injection level varies continuously with depth, z. In order to estimate an average volume density of injected carriers, a specific spatial averaging scheme must be adopted. Here, we define an average initial minority carrier density $\langle p\rangle$ for the layer by evaluating Eq. (3) at a specific average depth $\langle z\rangle$, determined by requiring that the same number of photons are absorbed in the range $0\le z\le\langle z\rangle$ as in the range $\langle z\rangle\le z\le d$. This is satisfied when $e^{-\alpha\langle z\rangle}=1/2(1+e^{-\alpha d})$, leading to an average initial injection level of

$$\langle p\rangle \cong \frac{1}{2}(1-R)\Phi_o\alpha(1+e^{-\alpha d}). \tag{A1}$$

Equation (A1) is a reasonable estimate to the average initial injection level when $\alpha d<1$, when there is a relatively small drop in transmitted light intensity across the layer. For $\alpha d>1$ this variation can become substantial, corresponding to a large gradient in the injected carrier concentration across the layer. Consequently, for very thick epilayers, $\langle p\rangle$ in Eq. (A1) is only a rough indicator of injection. For the samples studied here, $0.36\le\alpha d\le 0.70$.

The temperature-dependent injection level can be estimated using Eq. (A1) and the temperature dependence of the absorption coefficient at the 355 nm excitation wavelength. The latter has been measured by Galeckas *et al.*,[41] and the resulting $\alpha(T)$ is shown as the dotted line in Fig. 8. Between 250 and 650 K there is approximately a factor of 4 increase in α. Inserting $\alpha(T)$ into Eq. (A1) provides the change in average injection level with temperature, as shown in Fig. 8

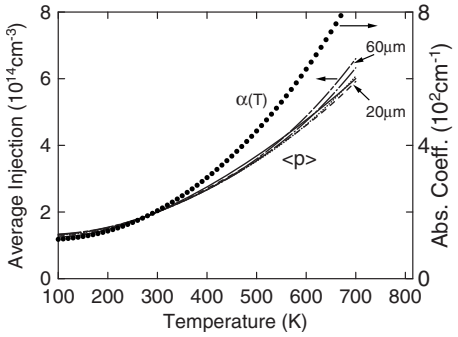

FIG. 8. Temperature dependence of the 355 nm absorption coefficient from Ref. 41 (dotted line), and of the average injection level from Eq. (A1) (solid and dashed lines) for layer thicknesses between 20 and 60 μm.

for layer thicknesses between 20 and 60 μm. The increase in α results in an increase in the injection level of about a factor of 3 over the entire temperature range.

We can obtain a sense of the impact that a three times increase in injection will have on measured carrier lifetimes through the measured injection level dependences of the lifetimes of samples NRL-1, NRL-2, and USC-3, which were shown in Fig. 3 for injection levels up to 2×10^{16} cm^{-3}. The dashed line represents the injection level at ≈250–300 K ($\approx2\times10^{14}$ cm^{-3}) and the dotted line indicates a three times increase (to 6×10^{14} cm^{-3}), simulating the increase in injection that would occur were the temperature raised to 650 K. From Fig. 3 it can be seen that this increase in injection corresponds to an increase in the carrier lifetime of ≤10%. This increase, distributed over the entire temperature range, is not considered to be sufficient to cause a serious distortion of the temperature-dependent carrier lifetimes, as the temperature variations that were observed are considerably larger than this.

[1]H. Matsunami and T. Kimoto, Mater. Sci. Eng. R. **20**, 125 (1997).
[2]P. Friedrichs, in *Silicon Carbide*, edited by P. Friedrichs, T. Kimoto, L. Ley, and G. Pensl (Wiley-VCH, Weinheim, 2010), Vol. 2, p. 21.
[3]M. Bhatnagar and B. J. Baliga, IEEE Trans. Electron Devices **40**, 645 (1993).
[4]K. Danno, D. Nakamura, and T. Kimoto, Appl. Phys. Lett. **90**, 202109 (2007).
[5]T. Kimoto, K. Danno, and J. Suda, Phys. Status Solidi B **245**, 1327 (2008).
[6]P. B. Klein, Phys. Status Solidi A **206**, 2257 (2009).
[7]P. B. Klein, B. V. Shanabrook, S. W. Huh, A. Y. Polyakov, M. Skowronski, J. J. Sumakeris, and M. J. O'Loughlin, Appl. Phys. Lett. **88**, 052110 (2006).
[8]J. Zhang, L. Storasta, J. P. Bergman, N. T. Son, and E. Janzén, J. Appl. Phys. **93**, 4708 (2003).
[9]S. A. Reshanov, W. Bartsch, B. Zippelius, and G. Pensl, Mater. Sci. Forum **615–617**, 699 (2009).
[10]L. Storasta, J. P. Bergman, A. Henry, E. Janzén, and J. Lu, J. Appl. Phys. **96**, 4909 (2004).
[11]T. Kimoto, A. Itoh, H. Matsunami, S. Sridhara, L. L. Clemen, R. P. Devaty, W. J. Choyke, T. Dalibor, C. Peppermüller, and G. Pensl, Appl. Phys. Lett. **67**, 2833 (1995).
[12]C. G. Hemmingsson, N. T. Son, A. Ellison, J. Zhang, and E. Janzén, Phys. Rev. B **58**, R10119 (1998).
[13]T. Kimoto, S. Nakazawa, K. Hashimoto, and H. Matsunami, Appl. Phys. Lett. **79**, 2761 (2001).
[14]W. Shockley and W. T. Read, Phys. Rev. **87**, 835 (1952).
[15]R. N. Hall, Phys. Rev. **87**, 387 (1952).
[16]R. K. Ahrenkiel, in *Semiconductors and Semimetals*, edited by R. K. Ahrenkiel and M. S. Lundstrom (Academic, New York, 1993), Vol. 39, pp. 39–150.
[17]J. Hassan and J. P. Bergman, J. Appl. Phys. **105**, 123518 (2009).
[18]E. Yablonovitch, D. L. Allara, C. C. Chang, T. Gmitter, and T. B. Bright, Phys. Rev. Lett. **57**, 249 (1986).
[19]D. J. Fitzgerald and A. S. Groves, Surf. Sci. **9**, 347 (1968).
[20]T. Saitoh and H. Hasegawa, Jpn. J. Appl. Phys., Part 2 **29**, L2296 (1990).
[21]Y. J. Shacham-Diamand and I. Kidron, Infrared Phys. **21**, 105 (1981).
[22]V. Grivickas, J. Linnros, and A. Galeckas, Mater. Sci. Forum **264–268**, 529 (1998).
[23]A. Galeckas, J. Linnros, M. Frischholz, and V. Grivickas, Appl. Phys. Lett. **79**, 365 (2001).
[24]M. Boulou and D. Bois, J. Appl. Phys. **48**, 4713 (1977).
[25]K. L. Luke and L.-J. Cheng, J. Appl. Phys. **61**, 2282 (1987).
[26]G. S. Kousik, Z. G. Ling, and P. K. Ajmera, J. Appl. Phys. **72**, 141 (1992).
[27]T. Otaredian, Solid-State Electron. **36**, 153 (1993).
[28]A. B. Sproul, J. Appl. Phys. **76**, 2851 (1994).
[29]R. K. Ahrenkiel and J. Dashdorj, J. Vac. Sci. Technol. B **22**, 2063 (2004).
[30]P. B. Klein, J. Appl. Phys. **103**, 033702 (2008).
[31]P. Grivickas, J. Linnros, and V. Grivickas, J. Mater. Res. **16**, 524 (2001).
[32]S. R. Dhariwal and D. R. Mehrotra, Solid-State Electron. **31**, 1355 (1988).
[33]S. J. Robinson, S. R. Wenham, P. P. Altermatt, A. G. Aberle, G. Heiser, and M. A. Green, J. Appl. Phys. **78**, 4740 (1995).
[34]A. G. Aberle, S. Glunz, and W. Warta, J. Appl. Phys. **71**, 4422 (1992).
[35]B. Adamowicz and H. Hasegawa, Jpn. J. Appl. Phys., Part 1 **37**, 1631 (1998).
[36]P. B. Klein, R. Myers-Ward, K.-K. Lew, B. L. VanMil, C. R. Eddy, Jr., D. K. Gaskill, A. Shrivastava, and T. S. Sudarshan (unpublished).
[37]A. Galeckas, J. Linnros, V. Grivickas, U. Lindefelt, and C. Hallin, Appl. Phys. Lett. **71**, 3269 (1997).
[38]V. K. Khanna, Prog. Quantum Electron. **29**, 59 (2005).
[39]R. J. Kingston and S. F. Neustadter, J. Appl. Phys. **26**, 718 (1955).
[40]G. W. 't Hooft and C. van Opdorp, Appl. Phys. Lett. **42**, 813 (1983).
[41]A. Galeckas, P. Grivickas, V. Grivickas, V. Bikbajevas, and J. Linnros, Phys. Status Solidi A **191**, 613 (2002).